Chip-Level GHz Capable Balanced Quantum Homodyne Receivers

Dinka Milovančev, *Member, IEEE*, Florian Honz, *Student Member, IEEE*, Nemanja Vokić, *Member, IEEE*, Martin Achleitner, Fabian Laudenbach, Christoph Pacher, Hannes Hübel, and Bernhard Schrenk, *Member, IEEE*

***Abstract*—We present a design of balanced homodyne receivers suitable for ultra-low noise quantum applications such as continuous-variable quantum key distribution and quantum random number generation. For best noise and bandwidth performance a die-level low-parasitic photodiode together with a low-noise high-speed transimpedance amplifier are explored together with a planar lightwave circuit splitter chip serving as a photomixer. Bandwidths of 750 MHz and 2.6 GHz were accomplished while maintaining optimum noise performance, as evidenced by very high quantum-to-classical noise ratios of 26.8 and 18.6 dB, respectively. A common-mode rejection ratio of at least 40 dB was achieved for a frequency range of up to 1 GHz. Its application for continuous-variable quantum key distribution was evaluated by means of estimations under a strict untrusted receiver assumption, showing its potential for generating up to 43 Mbit/s secure-key rate over a reach of 10 km, whereas up to 100 Mbit/s could be supported at shorter reaches. Moreover, the high quantum-to-classical clearance values can enable high quality quantum random number generation at Gb/s rates. The multi-purpose operation of the designed balanced receivers for classical communications was examined showing reception sensitivities of -55.8 and -52.6 dBm at 500 Mbit/s and 1 Gbit/s quadrature phase shift keying transmission, respectively, using the 750 MHz receiver. The faster 2.6 GHz receiver enabled 10 Gbit/s duobinary transmission at -14.8 dBm sensitivity.**

***Index Terms*—Optical signal detection, photodetectors, optical receivers, quantum communication, optical fiber communication, random number generation.**

I. Introduction

QUANTUM technologies are advancing towards technological maturity, prompting their employability and expanding their use cases. Data transfer and security can take advantage of the benefits offered by the quantum systems and protocols, especially with the rise of virtual services spanning from online banking to the transfer of sensitive medical data. The information-theoretic secure communication offered by quantum key distribution (QKD) is becoming more and more important in our growing digital society. QKD can address security challenges by exploiting the quantum-mechanic properties of light to exchange secret keys and encrypt data [1]. However, a few roadblocks are still to be overcome for QKD to be widely accepted. Small size, low-cost solutions that are easy to be integrated into existing infrastructure are some of the crucial points. The limited link budgets and co-existence with classical communication channels that require orders of magnitude higher launch levels are setting additional constraints [2]. The main challenge stems from the receiver side since it needs to resolve signal levels in the order of a single photon per bit, which is necessary to exploit quantum-mechanic effects. The two main approaches for quantum-encrypted transmission are discrete variable (DV-) and continuous variable (CV)-QKD. DV-QKD relies on single-photon avalanche photodiodes (SPAD) or superconducting nanowires single-photon detectors (SNSPD) which practically deliver a discrete (i.e., saturated) signal [3]. However, these devices

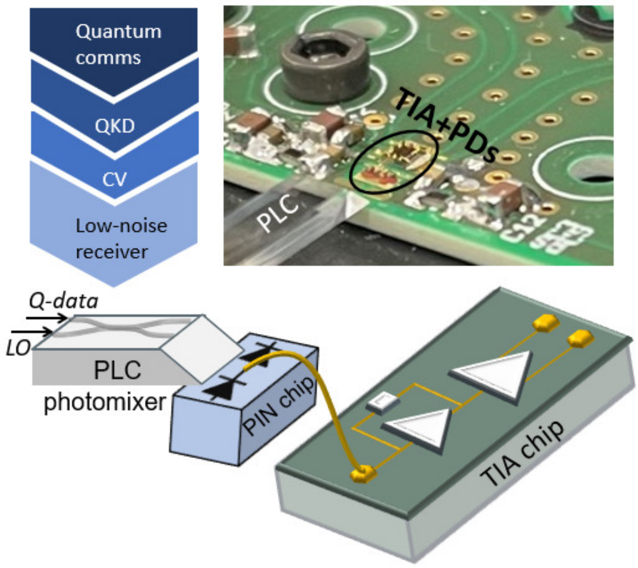

Fig. 1. Quantum Rx – die level subassembly: PLC splitter chip as photomixer and photodiode array chip wire-bonded to a low-noise TIA chip.

This Manuscript received May 31, 2022, revised September 28, 2022. This work was supported in part by the European Research Council (ERC) under the European Union's Horizon 2020 research and innovation programme (grant agreement No 804769) and by the Austrian Research Promotion Agency FFG through the EQUINOX project (grant agreement n° 884443).

D. Milovančev, F. Honz, N. Vokić, M. Achleitner, C. Pacher, H. Hübel and B. Schrenk are with the AIT Austrian Institute of Technology, Center for Digital Safety&Security, Giefinggasse 4, 1210 Vienna, Austria (phone: +43 50550-4131; fax: -4150; e-mail: dinka.milovancev@ait.ac.at).

F. Laudenbach is with Xanadu Quantum Technologies Inc., M5G 2C8, Toronto, Canada (e-mail: fabian@xanadu.ai).

come with a given degree of complexity such as a complex cooling system in case of SNSPDs (with a working temperature of 3-4 K), or a highly limited speed of operation (~100 MHz) due to the necessary dead-time of SPAD devices. The speed aspects, together with the low photodetection efficiency of SPADs at telecom wavelengths, make DV-QKD systems better suited for low data rates and longer reach [2,4,5]. DV-QKD is susceptible to Raman noise and requires a careful spectral allocation for co-existence with classical signals [6]. CV-QKD enables the quantum signal to have a continuum of values instead of a discrete alphabet. CV-QKD measures the quadrature field components of weak coherent states via coherent detection, which is aided by a powerful local oscillator (LO) to overcome the electrical noise of balanced homodyne detectors (BHD) [7,8]. Coherent detection also helps to tackle the co-existence challenge since the LO can be precisely tuned to the desired wavelength, thus rejecting out-of-band signals. Classical coherent systems are traditionally used for long-haul networks; however, recent industrial interest is driving the inclusion of coherent systems into short-reach networks [9], which also provides a good overlap with obtainable CV-QKD transmission reaches.

The workhorse of coherent detection is a BHD. For classical communications the target performance indicator of a BHD is its bandwidth. Although desirable from a communication capacity perspective, a large bandwidth comes with a caveat: it entails relatively high electrical noise if off-the-shelf high speed telecom BHDs are directly adopted. Therefore, optimization toward the low-noise regime is a necessity for quantum applications, while still preserving as much bandwidth as possible. For overcoming the electrical noise, we can use very high LO powers; however, the available LO power can be limited depending on the device performances or whether it is co-propagated with the quantum signal [10,11] making it susceptible to attenuation along the channel. Moreover, an excessive LO power may saturate the photodiodes, thus limiting further performance gains. This saturation limit is usually in the order of tens of mW. In [12] it is estimated that the noise of the electrical circuitry can amount up to 65 % of the total excess noise at the detector side, making it the biggest noise contributor for a typical CV receiver. This ultimately limits the reach and secure-key generation rate. Therefore, optimizing the electrical noise of a BHD promises high performance gains.

Most CV-QKD receivers reported so far used discrete electronics that are generally unable to efficiently cope with bandwidths exceeding 100 MHz while maintaining low noise levels. The reason is that discrete operational amplifiers (op-amps) with available gain-bandwidth (GBW) product of up to just a few GHz are used, which together with the high capacitance of printed circuit board (PCB) traces and bulky transistor outline (TO)-can packaged optical devices make for very constrained design choices. On the optics side, photonic integrated circuits (PIC) were introduced relatively recently for use in BHDs. Currently there is an ongoing exploration of PIC-based solutions together with co-designed electronics, offering record performances [13,14].

In this work we are using die-level componentry on the optical and electrical sides for realizing BHDs (Fig. 1). Instead of a dedicated custom PIC and custom electrical integrated circuit (IC) designs, we are exploring the potential of existing commercially available chip-level components for both photonic as well as electronic elements, thus minimizing the parasitics and achieving low-noise operation. This paper is the extension of our initial works [15,16] and covers the performance characterization of different designs of die-level photodiode / transimpedance amplifier (TIA) assemblies in search for optimum design trade-offs for BHDs in view of quantum applications.

This paper is organized as follows. Section II describes the design procedure of BHD receivers. Characterization of different BHD receiver architectures and their placement within the state-of-the-art is discussed in Section III. The applications of our BHD receivers in CV-QKD and QRNG domains are addressed in Section IV. Section V demonstrates the suitability of our multi-purpose BHDs for the reception of classical optical communication signals. Finally, Section VI concludes the work.

II. Design of BHD receivers

As indicated in Section I, the use of discrete componentry for BHDs limits the performance due to harsh trade-offs between gain and bandwidth. The equivalent input-referred noise current $i_{n,EQ}$ of a discrete TIA design based on operational amplifiers can be calculated as [17]:

$$i_{n,EQ} = \sqrt{i_n^2 + \frac{4kT}{R_F} + \left(\frac{e_n}{R_F}\right)^2 + \frac{(e_n 2\pi F C_{tot})^2}{3}} \quad (1)$$

where i_n is the op-amp equivalent current noise source, e_n is the op-amp equivalent input noise voltage source, R_F is the transimpedance gain corresponding to a feedback resistance, F presents the noise integration frequency limit for which a rough estimate can be taken up to the 3-dB bandwidth according to a brick-wall transfer function approximation, C_{tot} is the total input capacitance comprised of the PCB traces, photodiode and op-amp input capacitances. For optimum noise performance, R_F should be as large as possible for a target bandwidth BW_{3dB}; however, it is limited by the GBW of the operational amplifier [17]:

$$R_F \approx \frac{GBW}{(2\pi C_{tot} BW_{3dB}^2)} \quad (2)$$

Several different operational amplifiers with high GBW were considered. We assumed a value of 1 pF for the photodiode capacitance, which is a typical value for TO-can devices. The PCB trace capacitance was also supposed to be 1 pF. Figure 2 shows the calculated input-referred rms noise current $i_{n,rms}$ for the two target bandwidths of 250 MHz and 1 GHz. The noise performance drops significantly with increased bandwidth. Moreover, the achievable transimpedance gain also becomes quite low, which can lead to further increase of the overall noise if post-amplification is needed, since the noise of all the post-amplifying stages is being divided with R_F when referred to the input.

To minimize the parasitics, while still using commercially available components, we chose to use die-level components

TABLE I
INGAAS PIN CHIP PROPERTIES

Property/PD	PD1	PD2	PD3
Configuration	1x4 array	1x4 array	Single die
Pads	P/N P: ⌀ 80 µm N: 80x80 µm^2	GSG width 70 µm G: 2x S-area	P/N P: ⌀ 60 µm N: 60x165 µm^2
Data rate Rating/BW	10 Gb/s 12 GHz	25 Gb/s 22 GHz	10 Gb/s 10 GHz
Capacitance	0.16 pF	0.12 pF	0.22 pF
Active area	⌀ 45 µm	⌀ 20 µm	⌀ 50 µm
Responsivity @1550 nm	1 A/W	0.8 A/W	1.1 A/W

P/N – p-type doped and n-typed doped region electrodes for photodiode bias, GSG – ground signal ground electrodes, ⌀ – diameter

TABLE II
TIA CHIP PROPERTIES

TIA/Property	Transimpedance	Speed rating	BW_{3dB}	$i_{n,rms}$	Power consumption
TIA1	60 kΩ	1.25 Gb/s	860 MHz @ Cin=0.5 pF	60 nA @ (BWn = 940 MHz, Cin=0.5 pF)	181.5 mW
TIA2	3.2 kΩ	4.25 Gb/s	2.8 GHz @ Cin=0.2 pF	465 nA @ (BWn = 4 GHz, Cin=0.2 pF)	56.1 mW

BWn – noise bandwidth

for both photonic and electronic strata. PIN photodiode arrays suitable for 1550 nm are chosen such that their pitch corresponds to 250 µm so that it can be interfaced via vertical coupling with a glass photonic lightwave circuit (PLC) splitter chip for efficient photomixing (Fig. 1). The PLC-based approach enables a high coupling efficiency to the photodiodes that is hard to obtain on a PIC, as well as skew-free operation and a compact footprint, which is hard to obtain with bulk optics or fiber-based solutions for optical mixers. The characteristics of the chosen photodiodes are summarized in Table I. For all the chosen photodiode variants the photodiode capacitances (bonding pad + junction capacitance) are smaller than 250 fF. Therefore, the input capacitance is significantly reduced compared to discrete componentry since there are no packaging parasitics and no PCB trace parasitics. The issue of input capacitance is paramount for an optimum TIA noise performance, since even in a noise-optimized integrated TIA design the total input referred (rms) noise current will scale with $\sqrt{C_{PD}}$ [18].

Two options are considered for the TIA. The first is an ultra-

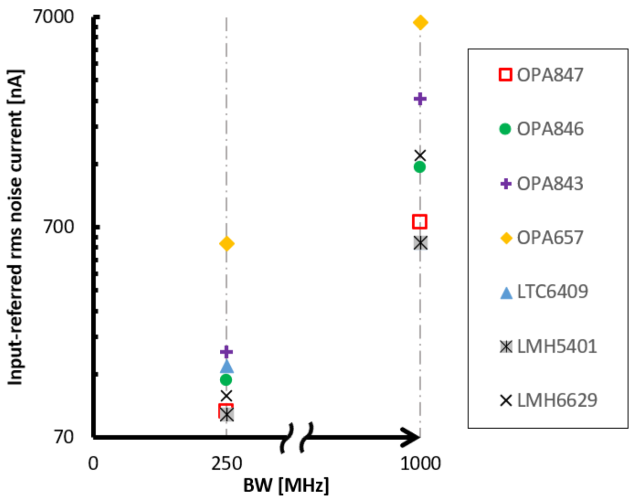

Fig. 2. Input-referred noise current of commercial op-amp based TIAs for target 3 dB bandwidths of 250 MHz and 1 GHz.

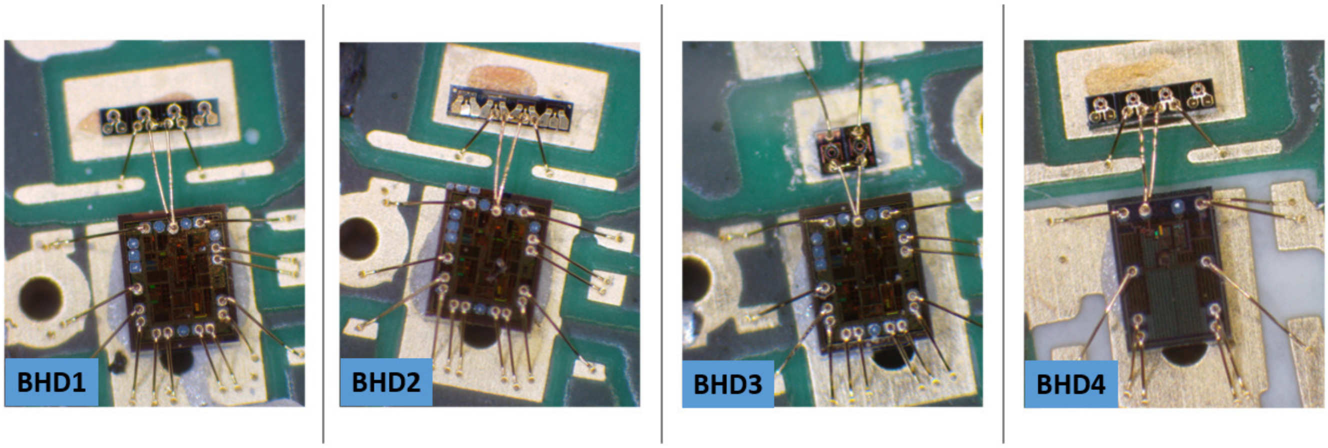

Fig. 3. Different combinations of photonic and electrical circuits for BHD die level subassembly: BHD1 (1x4 array of PDs with symmetric P/N pads +1.25 Gb/s TIA), BHD2 (1x4 array of PDs with GSG pads +1.25 Gb/s TIA), BHD3 (2 independent PD dies + 1.25 Gb/s TIA) and BHD4 (1x4 array of PDs with symmetric P/N pads +4.25 Gb/s TIA).

This article has been accepted for publication in IEEE/OSA Journal of Lightwave Technology. This is the author's version which has not been fully edited and content may change prior to final publication. Citation information: DOI 10.1109/JLT.2022.3211095

low noise TIA, denoted as TIA1, rated for 1.25 Gb/s with only 60 nA of $i_{n,rms}$ over a bandwidth of 940 MHz. The second, TIA2, targeted for a higher speed of 4.25 Gb/s and having an $i_{n,rms}$ of 460 nA over a bandwidth of 4 GHz. The main parameters of both TIAs are summarized in Table II. The achievable noise and gain performances for specified input capacitances are substantially better than what can be achieved with discrete componentry at higher bandwidths. Based on these available components, we have designed four different BHD receivers: BHD1 (PD1 + TIA1), BHD2 (PD2 + TIA1) and BHD3 (PD3 + TIA1). All of them featured the same low-noise TIA while the photonic interface has been changed. A high-speed BHD receiver was used in BHD4 (PD1+ TIA2), see Fig. 3. Each of the designed BHDs was laid out for being interfaced with the PLC-based photomixer.

III. Characterization of BHD Receivers

A. *Common-Mode Rejection Ratio*

For the initial characterization of the receivers, we first measured the common-mode rejection ratio (CMRR) for all four BHD variants. The CMRR is defined as the ratio of the difference current ΔI under dual photodiode illumination (i.e., the balanced case) versus the individual response of each photodiode corresponding to the illumination of a single photodiode (i.e., the unbalanced case). The response during the balanced and the unbalanced mode of operation is amplified by the TIA. Therefore, we measure the CMRR as the ratio of output voltages:

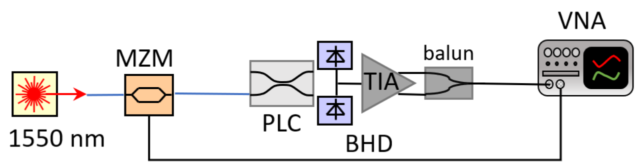

Fig. 4. CMRR measurement setup.

$$CMRR = 20\log_{10}\frac{V_{unbalanced}}{V_{balanced}}. \qquad (3)$$

The incident optical power during the measurement of the balanced and unbalanced cases needs to be kept at the same level and it should be low enough not to saturate the BHD during the unbalanced mode of operation. The CMRR strongly depends on the extent of photodiode matching, the topology of the electrical circuitry, and the splitting ratio of the employed optics used to guide the light to the photodiodes. Due to the frequency-dependent behaviors of the photodiode and the electrical circuitry, the CMRR becomes frequency dependent as well. To measure it over a wide frequency range, the setup depicted in Fig. 4 was used. The optical input was modulated via a Mach-Zehnder modulator (MZM) driven by one port of a vector network analyzer (VNA), whereas the BHD output was fed to the other VNA port to obtain the S-parameters of the receiver. A high CMRR value is desired since it indicates good rejection of the common-mode noise, reduction of relative intensity noise (RIN), the suppression of direct detection terms resulting from jointly co-propagated adjacent channels, as well as suppression of any dc current that might flow into the electrical circuitry, which in case of dc-coupled circuits can alter the optimum operating points and lead to non-linearities. For experimental CV-QKD systems it is desired that the CMRR is larger than 30 dB over the desired operating frequency range [19, 20].

The measurement results for all four BHD receivers are reported in Fig. 5. During the measurements the difference in splitting ratio for the PLC was compensated by a lateral alignment of the PLC in a set-and-forget manner. The best results are obtained for BHD1 and BHD4, which employed a photodiode array with almost symmetric anode and cathode pads. The photodiodes had an active area that allowed a high coupling ratio of 80-85%. The CMRR is highest for BHD4 since it uses the TIA with a low transimpedance gain, meaning that a small change in dc input current does not induce a strong

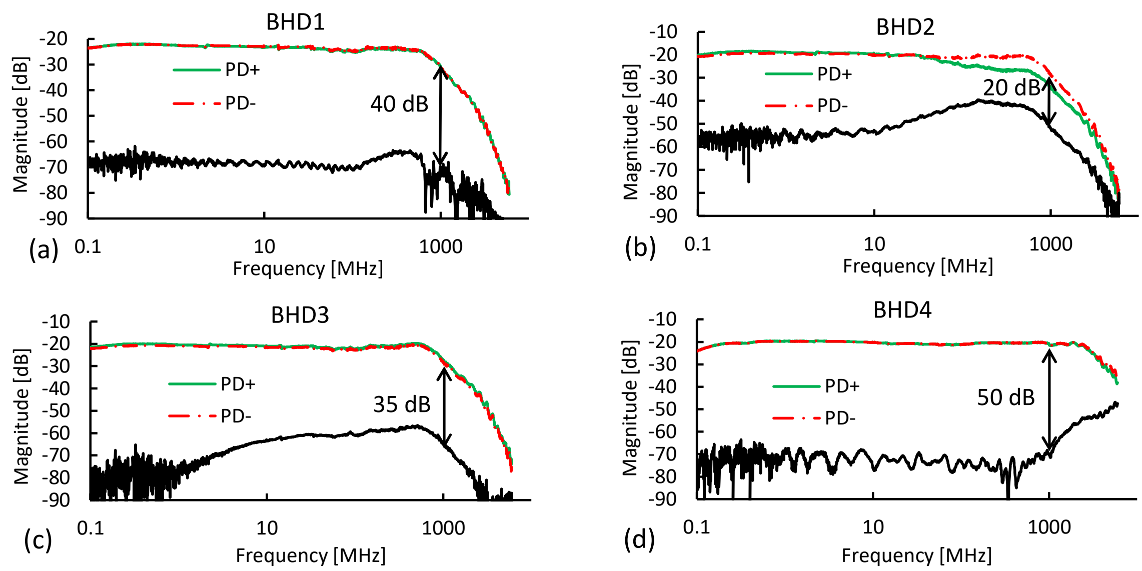

Fig. 5. CMRR measurement results of: (a) BHD1, (b) BHD2, (c) BHD3 and (d) BHD4.

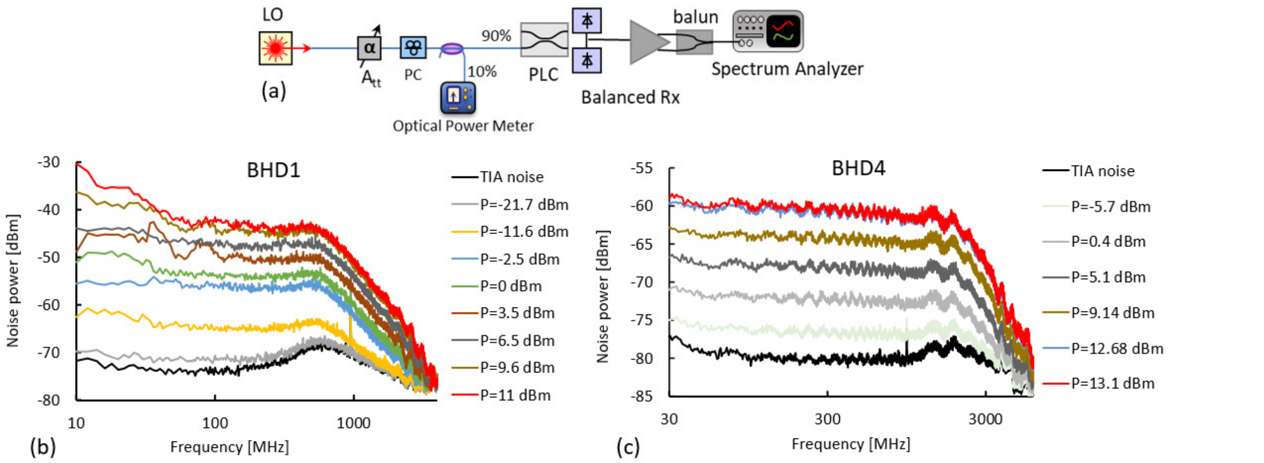

Fig. 6. Noise power measurements: (a) measurement setup, (b) noise power spectrum of BHD1, with –3 dB bandwidth of 700 MHz for highest input optical power, and (c) noise power spectrum of BHD4, with –3 dB bandwidth of 2.1 GHz for highest input optical power.

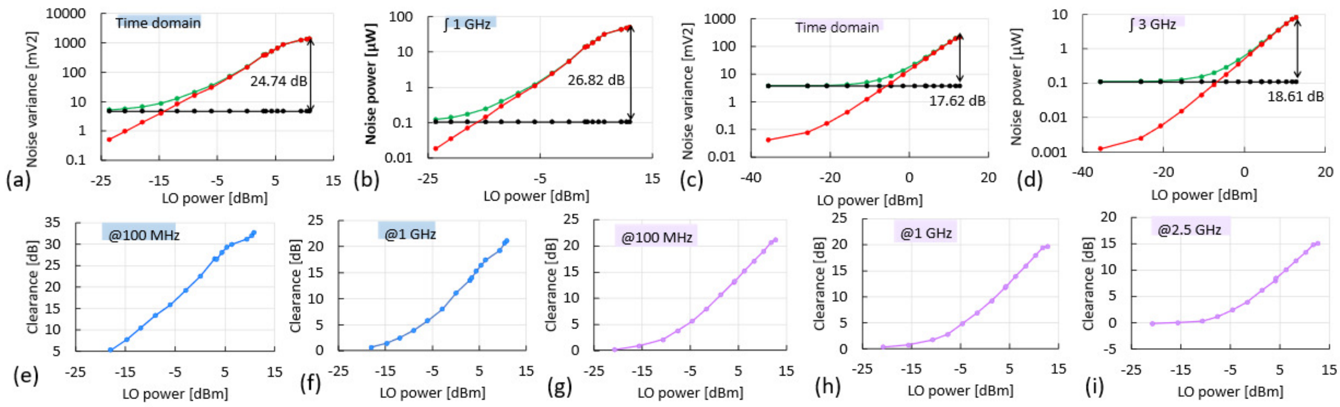

Fig. 7. QCNR measurements: (a) time domain BHD1, (b) frequency domain BHD1, (c) time domain BHD4, (d) frequency domain BHD4, and spot clearance at (e) 100 MHz BHD1, (f) 1 GHz BHD1, (g) 100 MHz BHD4, (h) 1 GHz BHD4, and (i) 2.5 GHz BHD4.

voltage offset at the output. A CMRR of 50 dB at 1 GHz was possible with BHD4, whereas BHD1 – due to its larger TIA gain – achieved 40 dB at 1 GHz. BHD3 uses a photodiode pair with rather asymmetric anode and cathode, where two separate photodiodes were placed tightly together to adhere to the pitch of the PLC. In this case, we see a lower CMRR compared to BHD1 and BHD4, reaching 40 dB at lower frequencies and 35 dB at 1 GHz. The coupling efficiency of BHD3 was 73 %, which is slightly reduced compared to BHD1 and BHD4 despite the large active area of 50 µm. This is attributed to the unfortunate position of the bondwires on the photodiodes, which prevented the PLC to approach closer to the photodiode chip. The measurements show the worst CMRR performance for BHD2 for which the CMRR drops by 10-20 dB after 100 MHz compared to its low-frequency value. This behavior is attributed to the G-S-G pad configuration (anode and cathode are quite asymmetric). On top of this, the high-speed capability (the PDs are rated for 25 Gb/s) could also contribute to a higher variability among photodiodes since the structures are considerably smaller and thus more sensitive to process variations. Due to the smaller aperture, the coupling efficiency was only 65% for BHD2.

B. Quantum-to-Classical Noise Ratio

The quantum-to-classical noise ratio (QCNR) is defined as the ratio of shot-noise variance (i.e., quantum noise) to the associated electrical and dark photocurrent noise variance (i.e., classical noise). Usually, it is estimated experimentally through the *clearance*, which is the ratio of total (observable) noise – optical input is present, as is the classical noise – to the case without optical input:

$$Clearance = 10\log_{10}\frac{\sigma^2_{n,total}}{\sigma^2_{n,clas}} = 10\log_{10}\frac{\sigma^2_{n,shot}+\sigma^2_{n,clas}}{\sigma^2_{n,clas}} \quad (4)$$

This quantum-to-classical noise clearance was evaluated for BHD1 and BHD4 receivers with highest coupling efficiency. The quantum noise estimation is an important measurement for CV-QKD systems as it influences the achievable secure-key rate over a given transmission distance, as well as the QRNG generation rate since this noise should dominate the classical noise. Therefore, the quantum noise should scale linearly with the optical power of the source laser (representing the LO). For quantum applications it is desired that the clearance remains above 10 dB [19], whereas recently reported advances indicate

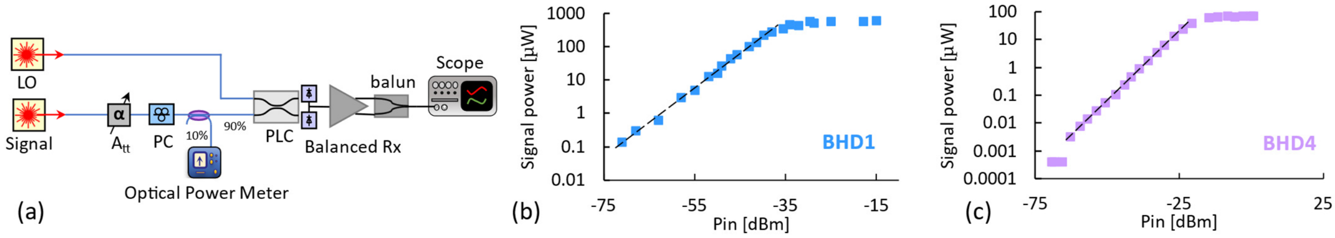

Fig. 8. TIA linearity measurement: (a) setup, (b) BHD1 linearity and (c) BHD4 linearity at LO power of 100 µW.

a shift in the performance requirement towards 20 dB [14].

Since we are estimating noise, the laser source is unmodulated and both photodiodes are illuminated as it is necessary for CV-QKD/QRNG measurements. Figure 6(a) shows the corresponding characterization setup. Figures 6(b) and 6(c) present the measured spectrum of the BHD receiver outputs for different LO powers. BHD1 can achieve more than 20 dB of clearance up to 1 GHz before its saturation, whereas BHD4 achieves more than 10 dB up to at least 3 GHz when measured with a spectrum analyzer. The BHD outputs were further recorded via a digital oscilloscope and subsequently postprocessed for QCNR estimation by subtracting the electronic noise from the total noise in both frequency and time domain. It should be noted that the noise due to analog-to-digital conversion of the real-time scope additionally contributes to the measured classical noise. In the frequency domain we integrated the spectrum from 1 MHz up to our bandwidth of interest (Figs. 7(b) and 7(d)), while in the time domain we estimated the time variance of the output BHD traces (Figs. 7(a) and 7(c)). The QCNR curves clearly show that the quantum noise is linearly increasing with the LO power for both BHD receivers. Although the same photodiode type is used, BHD1 clearly outperforms BHD4 due to lower electrical input-referred noise, even at the highest LO power levels where BHD4 cannot match BHD1. BHD1 can achieve a QCNR of 26.8 dB for a LO power of 12.3 mW, whereas BHD4 can achieve a QCNR of 18.6 dB at a LO power of 18.6 mW. In some works, the clearance value is reported for a single frequency (i.e., the spot clearance). Figure. 7 (e) and 7(f) present the spot clearance values at 100 MHz and 1 GHz. BHD1 can achieve very high clearance of 32.7 dB at 100 MHz and 21.1 dB at 1 GHz for the highest LO power. BHD4 can achieve a clearance of 21.1 dB at 100 MHz, 19.7 dB at 1 GHz and 15 dB at 2.5 GHz (Figs. 7(g), 7(h) and 7(i)).

C. *TIA Linearity*

The linearity is an important parameter for CV-QKD systems where complex analog modulation waveforms are used. Sufficient TIA linearity is required for high-fidelity opto-electrical conversion of such analog waveforms. The linearity depends on the magnitude of the input signal. Even though boosted by the LO, the expected quantum signal levels are still relatively weak, but strong pilot tones can exist for synchronization and LO training [21], which means that TIAs of sufficiently high linearity need to be employed. To determine the linearity range, a single tone was produced by heterodyne beating of two lasers, including a probe laser with variable output power and a LO laser set for a fixed power of 100 µW (Fig. 8(a)). Based on the linearity curve for P_{LO} = 100 µW, we can estimate the maximum permissible signal levels for different LO power values, since the quantum signal after mixing with the LO is proportional to $\sqrt{P_{LO}P_{sig}}$. Figure 8(b) shows the results for BHD1, where the beat note was set to 120 MHz. The saturation-free region spans from -71 up to -38 dBm of input signal power, yielding a dynamic range of 33 dB. BHD4 has an improved linearity region of 42.3 dB, spanning from -62.8 to -20.5 dBm of input signal power (Fig. 8(c)). This expanded linearity range of BHD4 can be expected due to its lower transimpedance gain; however, it comes at the cost of a worsened noise performance.

D. *State-of-the-Art in Balanced Receivers*

Table III summarizes some of the most important results in BHD designs. First designs of BHD receivers relied on bulk components and fiber optics for the photonic part and discrete components for electronics, thus limiting them in achievable bandwidth. Additionally, it becomes challenging to achieve a high CMRR over an extended frequency range due to photodiode mismatch and fiber split ratios, as well as time skew due to unequal optical path lengths. Usually, the bandwidths using discrete componentry are limited to less than 100 MHz [22-25] due to a high level of electronic noise at higher frequencies, which trades off with the available bandwidth and gain. Using discrete op-amp based TIAs, the highest bandwidths of 250 [26] and 300 MHz [27] were possible. The bandwidth enhancement was possible due to a two-stage amplification topology. The highest reported bandwidth using discrete componentry is 1.2 GHz [28]. This was possible since the photodiodes were loaded with 50Ω matching resistors for interfacing them with a voltage amplifier. However, 50Ω low-impedance front-ends suffer from high input-referred noise, which leaves room for design improvement. This receiver could reach up to 18.5 dB of clearance (integrated up to 1.2 GHz) at 8.1 mW of LO power. In contrast, BHD1 at a similar power of 8.7 mW can reach a value of 26 dB (integrated over 1 GHz) due to a better noise performance for its electrical front-end. The highest clearance value using discrete electronics is 37 dB, but at only 2 MHz and a very high optical input power of 54 mW [22]. The CMRR is usually improved by a careful selection of photodiodes, in an attempt to find a pair with the best matching in terms of capacitance, responsivity and frequency response. In these highly custom designs an additional degree of freedom is the bias voltage of the photodiodes used to further tweak their characteristics. In [22] a differential fine-tuning network was implemented to further improve the matching of photodiodes by eliminating the series resistance mismatch, thus extending the CMRR from 20 dB to 75.2 dB.

TABLE III
STATE OF THE ART – BHDS FOR QUANTUM APPLICATIONS

			Quantum receiver parameters						
Ref.	**Photonics**	**CV-QKD / QRNG BHD elements**	**BW$_{3dB}$**	**Clearance**		**P$_{LO}$ /I$_{PD}$**	**CMRR**		**Optical coupling eff. / loss at Rx**
				dB	*f*		dB	*f*	
This work [15,16]	Chip/die level PDs	Rx: PLC + InGaAs PIN + TIA die	750 MHz	32.7	@100 MHz	12 mW	40	≤ 1 GHz	85% Coupling efficiency
				26.82	∫1 GHz				
			2.6 GHz	21.1	@100 MHZ	18.6 mW	50	≤ 1 GHz	
					∫3 GHz				
[14]	SOI	Rx (PIC + custom TIA die)	1.5 GHz	28	@100 MHz	-/ (I_{PD} = 3.14 mA)	80	100 MHz	-
				>20	@1.5 GHz		>40	1.5 GHz	
[32]	SOI	QRNG Rx (SOI+hybrid InGaAs PDs +10bit – ADC - 2.5GSa/s), butterfly packaged		<10	∫1.2-3.2 GHz	3.36 mW	-		8.5 dB transmission loss
[29]	SOI	QRNG Rx (PIC + discrete electronics)	20 MHz	<10	10 MHz	10 mW	-		-
[13]	SOI	Rx (PIC + commercial TIA die)	1.7 GHz	14	∫1.7 GHz	4.36 mW	52	1	-2.1 dB (62%) coupling loss
[30]	SOI	Rx (PIC + discrete el.)	1-10 MHz	5	1-3 MHz	>10 mW	-		5 dB total loss
[31]	SOI	QRNG Rx (PIC + discrete electronics)	150 MHz	11	∫150 MHz	4.5 mW	28	50 MHz	-
[28]	TO-can PDs	Discrete el.: LNA + PDs + fiber optics	1.2 GHz	18.5	∫1.2 GHz	8.08 mW	57.9	50 MHz	-
[27]	TO-can PDs	Discrete el. (op-amp TIA + PDs) + bulk optics	300 MHz	14	300 MHz	6.13 mW	54	100 MHz	-
[26]	TO-can PDs	Discrete el. (op-amp TIA + PDs) + fiber optics	250 MHz	16.3	∫0-70 MHz	6.8 mW	52	100 MHz	-
[22]	TO-can PDs	Discrete el. (op-amp TIA + PDs) + bulk optics	5 MHz	37	@2 MHz	54 mW	75.2	2 MHz	-

Marked improvements in BHD performance were seen after adoption of chip-based solutions. First designs used only integrated photonics and discrete electronics [29-31] and thus still suffered from high associated noise and a limited bandwidth. Recently, a PIC wire-bonded to a commercial TIA [13] and a PIC having a dedicated TIA design [14] were reported. The high CMRR values accomplished in these works derive from a balancing function realized on-PIC, where MZMs are used to level out any waveguide splitting or photodiode responsivity mismatch. High clearance levels of more than 20 dB at 1 GHz, with maximum of 28 dB at 100 MHz, are reported in [14].

As can be seen regarding clearance values, our die-level solution compares well to the state-of-the-art since the input capacitance is mainly dominated by bonding pads that are necessary in both PIC based solutions, as well as vertically-coupled photodiode chips. BHD1 can achieve a spot clearance of 21.1 dB at 1 GHz, whereas at lower frequencies (100 MHz) it has a maximum clearance of 32.7 dB. The results of BHD4 are not as high in clearance values but still comparable to [13], where a clearance of 14 dB was achieved over 1.7 GHz at a LO power of 4.4 mW. At a similar LO power of 4.2 mW, BHD4 can achieve 13.3 dB of clearance over a wider range of 3 GHz. Regarding CMRR, higher values can be obtained by using fully PIC-based solutions since the PLC splitter is purely passive and the CMRR depends on an assembly-level alignment and the accuracy of its splitting ratio. The coupling efficiencies for both approaches, as well as the alignment difficulty and prospect of having a packaged solution, still need to be leveraged.

IV. PERFORMANCE FOR CV-QKD AND QRNG OPERATION

A. *BHDs for CV-QKD*

As an initial estimation of the BHD performance in CV-QKD, system simulations were performed. Simulations are based on the work in [12] and take as an input the measured characterization data of BHD1, since it features the best noise performance as desired for a CV-QKD receiver. The receiver excess noise is converted to shot-noise units (SNU) for which it translates to a very low value of 0.00336 SNU. A channel loss of 0.23 dB/km was chosen, which is the maximum attenuation of standard single-mode fiber at 1550 nm. Other loss sources

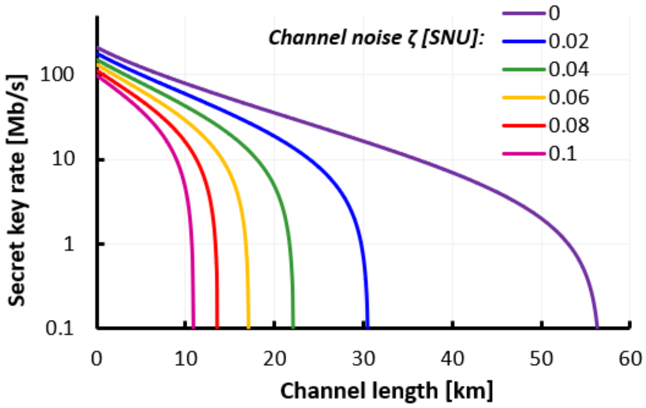

Fig. 9. CV-QKD performance simulation: secure-key rate vs. transmission distance based on the noise characteristics of BHD1 under untrusted receiver scenario.

that were considered are the net responsivity that includes a photodiode responsivity as well as vertical coupling losses, and the excess loss of the 180° hybrid (i.e., the PLC-based 3-dB splitter) necessary for photomixing of the quantum signal and the LO. These result in a total detection loss of 1.2 dB. For security analysis, an asymptotic secure-key rate is considered under the assumption that an infinite number of symbols is being transmitted, whereas the reconciliation efficiency between the two communicating parties, Alice and Bob, is 0.97. Since we are using an optical 180° mixer, a homodyne-detection protocol is assumed during this analysis. The transmission rate was 250 Mbaud under Gaussian modulation. The modulation variance was dynamically optimized to maximize the simulated key rate. Figure 9 shows the estimated secure-key rate as a function of the transmission distance, parametrized by the channel noise ζ. The channel noise is referred to the receiver input, meaning that it is already attenuated by the channel loss and no additional channel noise reduction is expected. The results of the simulations considered the untrusted receiver scenario, which is a more stringent security scenario, meaning that the excess noise of the electrical circuitry is considered when estimating the total excess noise, thus influencing the value of secret key rate (SKR). For reach of up to 10 km and $\zeta = 0.04$ SNU, a high SKR of 43 Mbit/s can be expected. Below 10 km, meaning an application domain for short reach scenarios, a very high SKR of 100 Mbit/s is expected, whereas over long reaches in the range of 30 km and a very low channel excess noise of 0.02 SNU we can expect a SKR of 1 Mbit/s.

B. BHD-Based Quantum Random Number Generation

Quantum random number generation is needed for achieving the highest levels of effectiveness in encryption methods, thus offering the desired security standards. Our BHD CV-QKD receivers may be re-used as random number generators by measuring vacuum-noise fluctuations. To evaluate the quality of randomness of the BHD output when it is used for measuring the vacuum fluctuations of an optical field using an unmodulated LO as a seed, an off-line digital signal processing (DSP) was performed. The outputs of both BHDs were acquired with a real-time oscilloscope having a resolution of 8 bits and a sampling rate of 20 GSa/s. The sampled data was then postprocessed using the universal Toeplitz hashing algorithm [33]. This algorithm improves the quality of the sampled data by shortening the raw data using an external random seed. By doing so, it corrects for randomness non-uniformity caused by correlations originating from a non-ideal TIA transfer function or any form of optical or electrical crosstalk including disturbances due to electro-magnetic interference. Therefore, the seeded randomness extraction algorithm improves the entropy per bit of the sampled data at the expense of shortening

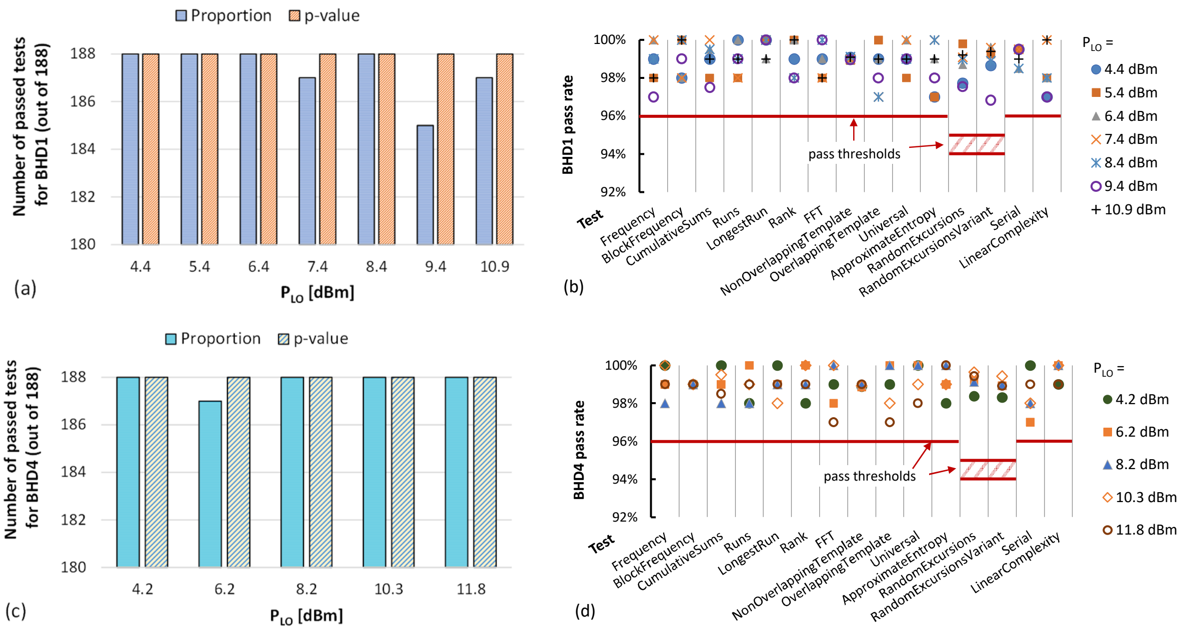

Fig. 10. NIST test results of sampled data showing the number of passing proportion and p-value tests for (a) BHD1 and (c) BHD4 receiver, as well as pass rate for each test group for (b) BHD1 and (d) BHD4 receiver.

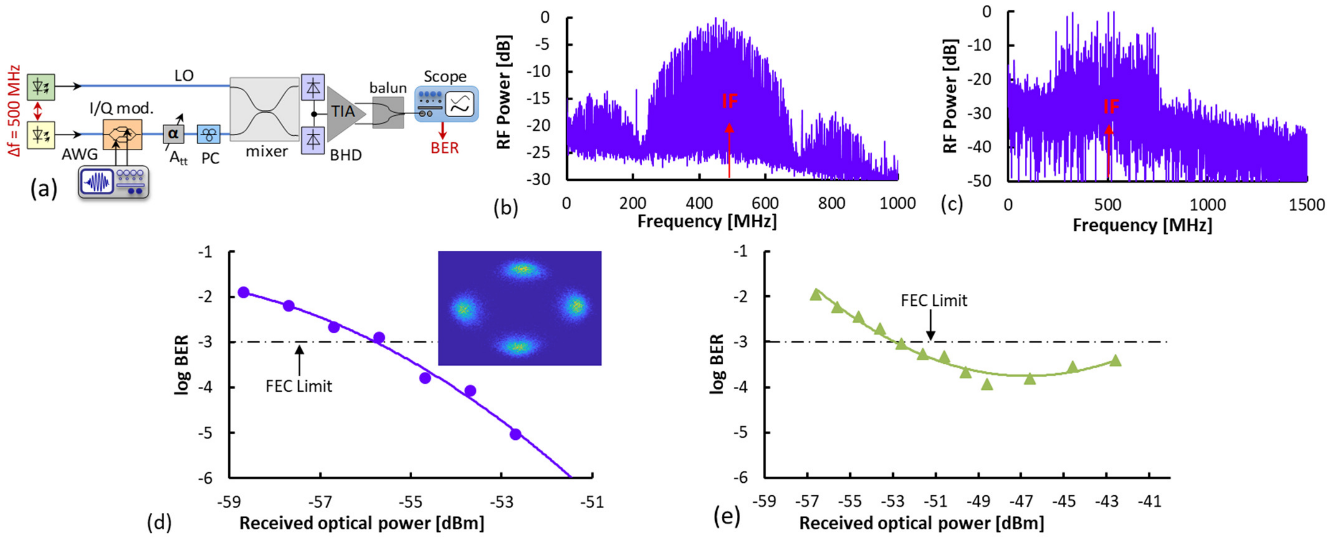

Fig. 11. Heterodyned QPSK coherent detection: (a) measurement setup, (b) spectrum for 250 Mbaud Gaussian, (c) spectrum for 500 Mbaud Nyquist shaped and BER vs. receiver optical signal power for (d) 250 Mbaud (Gauss) and (e) 500 Mbaud (Nyquist).

the random bit stream length. The ratio of output to input (O/I) data of the Toeplitz hashing was set to be 0.1. The hashed output consisting out of 100 sampled sets, each with a length of 10^6 bits, was examined via the randomness test suite NIST SP800-22-rev1a [34]. The results of these NIST tests for both, BHD1 and BHD4, are reported in Fig. 10. The generated random bit streams from the BHD outputs at different LO powers have passed all the NIST tests with respect to the uniformity of p-values as well as the number of sequences required to pass each NIST test. Due to its wider bandwidth, BHD4 features the highest QRNG rate, based on the conservative lower bound of the min-entropy of 1/10 bit per acquired bit and the used sampling rate of 20 GSa/s with an 8-bit resolution. We can have a QRNG rate of approximately 16 Gb/s, which translates to generating 62.5×10^6 256-bit advanced encryption standard (AES) keys. This high AES key rate would, however, require very fast analog-to-digital converters (ADCs) for real-time operation. A more modest estimation of the QRNG performance could be assessed by sampling at twice the bandwidth of interest (Nyquist rate). For a QRNG, the bandwidth of interest should be taken based on the clearance characteristics, i.e., up to the point where the total noise is larger than the classical noise. At the highest optical power values of the LO, the 3-dB clearance bandwidth is 3.6 GHz in case of BHD1, whereas in case of BHD4 it extends up to 6 GHz, which resembles the bandwidth of the used spectrum analyzer. These 3-dB clearance bandwidths would require sampling rates of 7.2 GSa/s and 12 GSa/s, respectively. Assuming again the conservative min-entropy value of 0.8 bits/sample, the QRNG rate would be 5.76 Gb/s (22.5×10^6 256-bit AES keys/s) using BHD1 and 9.6 Gb/s (37.5×10^6 256-bit AES keys/s) using BHD4.

V. Re-use as a Classical Communication Receiver

The two most promising balanced receivers for quantum applications, BHD1 and BHD4, can also have a dual-purpose role by enabling the data transfer for classical communications during quantum operation when quantum data transfer is idle. BHD1 has an excellent noise performance, but not for the highest bandwidth. Therefore, an attractive option is to exploit it together with advanced modulation formats enabled by coherent detection. Coherent communication is becoming more popular due to increased demands for higher data rates and spectral efficiency, as well as an optimal use of precious spectrum. The PLC + BHD1 front-end can therefore be utilized for simplified heterodyne coherent communication where a simple 180° optical hybrid is used as photomixer instead of a complex 90° hybrid. The demodulation of the in-phase (I) and quadrature (Q) components in case of a heterodyne scheme can then be off-loaded to the DSP. The bandwidth of BHD1 allows up to 1 Gb/s of unshared data rate per user. The coherent heterodyne data transmission setup is shown in Fig. 11(a). Two independent lasers, the signal laser and the LO, were beating at the intermediate frequency (IF) of 500 MHz. The signal laser was modulated via an optical I/Q modulator with QPSK data at 250 Mbaud using Gaussian pulse shaping (Fig. 11 (b)), as well as Nyquist pulse shaping (Fig. 11(c)) for an increased symbol rate of 500 Mbaud. The corresponding sensitivity is presented

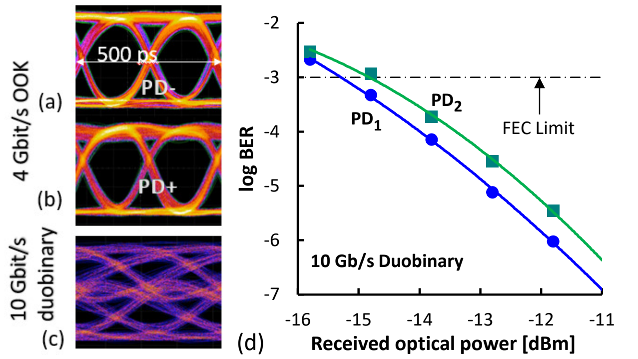

Fig. 12. BHD4 as GbE receiver: (a) eye diagram 4 Gbit/s OOK using PD-, (b) eye diagram 4 Gbit/s OOK using PD+, (c) eye diagram 10 Gbit/s duobinary and (d) sensitivity vs. input signal power at 10 Gbit/s duobinary, measured at individual photodiodes.

in Figs. 11 (d) and 11(e). The BHD1 receiver reached sensitivity of -55.8 dBm at 250 Mbaud and -52.6 dBm at 500 Mbaud for operation at the hard-decision forward error correction (FEC) threshold of $1\cdot10^{-3}$. The received spectra for the transmitted data clearly show the IF as well as the receiver bandwidth occupied by the data signal (Figs. 11(b) and 11(c)). The achieved sensitivities would allow optical budgets of 49.8 dB at 250 Mbaud and 44.6 dBm at 500 Mbaud, considering a typically low transmitted launch power of -6 dBm/λ from the central office located at the head-end of the communication link. The achieved sensitivities match well with state-of-the-art performances of highly sensitive coherent access receivers, such as reported in [35] with a sensitivity of -53 dBm at 311 Mbit/s, or [36] which achieves a sensitivity of -49.3 dBm at 1.25 Gbaud.

BHD4 with its bandwidth of 2.6 GHz can allow for a higher data rate. Besides QRNG operation, it can be re-used for GbE reception. QRNG operation could be accomplished in parallel with classical communications by utilizing unused photodiodes from a 1×4 array for direct detection. This is demonstrated by the wide-open eye diagrams at 4 Gbit/s on-off keying (OOK), as evidenced through Figs. 12(a) and 12(b), where 120 µA of current is being either sourced or sinked through the photodiodes used in a single-ended fashion. To improve the data rate further, duobinary modulation has been employed (Fig. 12(c)), for which the opto-electronic transfer function of the BHD serves as a low-pass filter for pulse shaping. The receiver bandwidth follows a 5th order Bessel function, for which the 3-dB bandwidth of 2.6 GHz is well-suited for 10 Gb/s duobinary operation [37]. The bit error ratio (BER) performances for each of the BHD photodiodes being illuminated separately are shown in Fig. 12(d). A sensitivity of -14.8 dBm is possible below the FEC limit of $1\cdot10^{-3}$.

VI. Conclusion

We presented main design constrains and performance indicators of balanced homodyne receivers. A series of characterizations revealed that a high performance comparable to a custom designed solution, can be achieved when using commercial die-level componentry. The high performance was also validated through estimations for CV-QKD and QRNG applications. Additionally, the re-use of quantum BHDs for classical communications was experimentally evaluated, showing excellent sensitivities. These open vistas for extended reach or optical loss budget using coherent detection, or higher data rates using duobinary modulation.

References

[1] R. Alléaume *et al,* "Using quantum key distribution for cryptographic purposes: A survey," Theor. Comp. Science, vol. 560, part 1, pp. 62-81, 2014.
[2] B. Fröhlich *et al*., "Long-distance quantum key distribution secure against coherent attacks," OSA Optica, vol. 4, no. 1, pp. 163-167, Jan. 2017.
[3] F. Ceccarelli *et al*., "Recent Advances and Future Perspectives of Single-Photon Avalanche Diodes for Quantum Photonics Applications", Adv. Quantum Technologies, vol. 4, no. 2, pp. 2000102, Feb. 2021.
[4] A. Boaron *et al*., "Simple 2.5 GHz time-bin quantum key distribution," Appl.Phys. Lett., vol. 112, no. 17, pp.171108, Apr. 2018.
[5] A. Boaron *et al*., "Secure Quantum Key Distribution over 421 km of Optical Fiber, " Phys. Rev. Lett., vol. 121, no. 19, pp. 190502, Nov. 2018.
[6] D. Zavitsanos *et al*., "Coexistence of Discrete-Variable QKD with WDM Classical Signals in the C-Band for Fiber Access Environments," 21st Int. Conf. Transparent Opt. Netw. (ICTON), Angers, France, Jul. 2019, paper Th.A5.4
[7] E. Diamanti and A. Leverrier, "Distributing Secret Keys with Quantum Continuous Variables: Principle, Security and implementations", Entropy, vol. 31, no. 9, pp. 6072-6092, Aug. 2015.
[8] S. Pirandola et al., "Advances in Quantum Cryptography", Adv. Opt. Photon., vol. 12, no. 4, pp.1012-1236, Dec. 2020.
[9] X. Pang *et al*., "High-Speed Short Reach Optical Communications: Technological Options and Challenges, " 2020 Asia Commun. Photonics Conf., Beijing, China, Mar. 2020, paper S3H.5.
[10] P. Jouguet et al., "Experimental demonstration of long-distance continuous-variable QKD", Nature Phot., vol. 7, no. 5, pp. 378-381, Apr. 2013.
[11] B. Qi et al., "Experimental study on the Gaussian-modulated coherent state quantum key distribution over standard telecommunication fibers", Phys. Rev. A, vol. 76, no. 5, pp.052323, Nov. 2007.
[12] F. Laudenbach et al., "Continuous-Variable Quantum Key Distribution with Gaussian Modulation – The Theory of Practical Implementations", Wiley Adv. Quantum Tech., vol. 1, no.1, pp. 1800011, Aug. 2018.
[13] J.F Tasker et al. "Silicon photonics interfaced with integrated electronics for 9 GHz measurement of squeezed light", Nat. Photonics, vol.15, no.1, pp. 11-15, Nov. 2021.
[14] C. Bruynsteen *et al.*, "Integrated balanced homodyne photonic–electronic detector for beyond 20 GHz shot-noise-limited measurements," Optica, vol 8, no. 9, pp. 1146-1152, Sep. 2021.
[15] D. Milovančev *et al.*, "Ultra-Low Noise Balanced Receiver with >20 dB Quantum-to-Classical Noise Clearance at 1 GHz," in *Proc. Europ. Conf. Opt. Comm.*, Bordeaux, France, Sep. 2021, paper TH2.D
[16] F. Honz *et al.*, "Broadband Balanced Homodyne Detector for High-Rate (>10 Gb/s) Vacuum-Noise Quantum Random Number Generation, " in Proc. Europ. Conf. Opt. Comm., Bordeaux, France, Sep. 2021, paper TU3G.
[17] X. Ramus, "Transimpedance Considerations for High Speed Amplifiers," Texas Instruments, USA, Application report - SBOA122, Nov. 2009.
[18] E. Säckinger, "Analysis and Design of Transimpedance Amplifiers for Optical Receivers," Hoboken NJ, Wiley, 2017
[19] Q. Zhou, "Design and application of low-noise, broadband photo-detector in quantum optics," PhD thesis, Shanxi University, Taiyuan, China, 2010.
[20] Y. Chi et al., "A balanced homodyne detector for high-rate Gaussian-modulated coherent-state quantum key distribution," IOP New J. Phys., vol. 13, no. 1, pp. 013003, Jan. 2011.
[21] D. Milovančev, N. Vokić, F. Laudenbach, C. Pacher, H. Hübel, and B. Schrenk, "High Rate CV-QKD Secured Mobile WDM Fronthaul for Dense 5G Radio Networks," IEEE J. of Lightw. Technol., vol. 31, no. 11, pp. 3445-3457, Jun. 2021.
[22] X. Jin et al., "Balanced homodyne detection with high common mode rejection ratio based on parameter compensation of two arbitrary photodiodes," OSA Opt. Expr., vol. 23, pp. 23859-23866, Sep. 2015.
[23] J. Appel et al., "Electronic noise in optical homodyne tomography," Phys. Rev. A, vol. 75, pp. 035802, Mar. 2007.
[24] O.M. Haderka et al., "Fast time-domain balanced homodyne detection of light," Appl. Opt., vol. 48, p. 2884, May 2009.
[25] R. Kumar *et al*., "Versatile wideband balanced detector for quantum optical homodyne tomography," Opt. Comm., vol. 285, no. 24, pp. 5259-5267, Nov. 2012.
[26] Q. Lu et al., "Ultra-Low-Noise Balanced Detectors for Optical Time-Domain Measurements," IEEE Trans. Nuclear Science, vol. 66, no. 7, pp. 1048-1055, Jul. 2019.
[27] D.F. Huang et al., "A 300-MHz Bandwidth Balanced Homodyne Detector for Continuous Variable Quantum Key Distribution", Chinese Phys. Lett., vol. 30, no. 11, p. 114209, Nov. 2013.
[28] X. Zhang et al., "1.2-GHz Balanced Homodyne Detector for Continuous-Variable Quantum Information Technology," IEEE Phot. J., vol. 10, no. 5, pp. 1-10, Oct. 2018.
[29] Z.Menglin et al., "1.2-GHz Balanced Homodyne Detector for Continuous-Variable Quantum Information Technology," J. Phys. Conf. Ser., vol. 1865, pp. 022018, Apr. 2021
[30] G. Zhang, et al. "An integrated silicon photonic chip platform for continuous-variable quantum key distribution," *Nat. Photonics,* vol. 13, no 12, pp. 839–842, Aug. 2019.

[31] F. Raffaelli *et al*., "A homodyne detector integrated onto a photonic chip for measuring quantum states and generating random numbers," Quantum Sci. Technol., vol. 3, no. 2, pp. 025003, Feb. 2018
[32] B. Bai et al., "18.8 Gbps real-time quantum random number generator with a photonic integrated chip, " Appl. Phys. Lett., vol. 118, no. 26, pp. 264001 2021.
[33] Y. Mansour, N. Disan, and P. Tiwari, "The computational complexity of universal hashing", Theor. Comp. Science, vol. 107, no. 1, pp. 121-133, Apr. 1993.
[34] L.E. Bassham et al., "A Statistical Test Suite for Random and Pseudorandom Number Generators for Cryptographic Applications", NIST special publication 800-22, Revision 1a, National Institute of Standards and Technology, 2010.
[35] S. Smolorz et al., "Demonstration of a Coherent UDWDM-PON with Real-Time Processing," in Proc. Opt. Fib. Comm. Conf. (OFC), Los Angeles, United States, Mar. 2011, PDPD4.
[36] A. Shahpari et al., "Coherent access:Areview," J. Lightw. Technol., vol. 35, no. 4, pp. 1050–1058, Feb. 2017.
[37] M. Omella et al., "10 Gb/s RSOA Transmission by Direct Duobinary Modulation", in Proc. Europ. Conf. Opt. Comm. (ECOC'08), Brussels, Belgium, Sep. 2008, vol. 2, pp. 123-124.